Experimental study of Gamow-Teller transitions via the high-energy-resolution ^{18}O(^{3}He,t)^{18}F reaction: Identification of the low-energy “super” -Gamow -Teller state

H. Fujita *et al.*

Phys. Rev. C **100**, 034618 — Published 26 September 2019

DOI: 10.1103/PhysRevC.100.034618

Study of Gamow-Teller transitions via high energy-resolution ^{18}O(^{3}He,t)^{18}F reaction — Identification of the Low-energy Super-Gamow-Teller state —

H. Fujita,[1,*] Y. Fujita,[1,2] Y. Utsuno,[3] K. Yoshida,[4] T. Adachi,[1] A. Algora,[5,6] M. Csatlós,[6] J.M. Deaven,[7,8,9] E. Estevez-Aguado,[5] C.J. Guess,[7,8,9,†] J. Gulyás,[6] K. Hatanaka,[1] K. Hirota,[1] R. Hutton,[7,8,9,‡] D. Ishikawa,[1] A. Krasznahorkay,[6] H. Matsubara,[1,§] F. Molina,[5,¶] H. Okamura,[1,**] H.J. Ong,[1] G. Perdikakis,[7,8,9] B. Rubio,[5] C. Scholl,[10,††] Y. Shimbara,[11,‡‡] G. Süsoy,[1,12] T. Suzuki,[1] A. Tamii,[1] J.H. Thies,[13] R.G.T. Zegers,[7,8,9] and J. Zenihiro[1,§§]

[1]*Research Center for Nuclear Physics, Osaka University, Ibaraki, Osaka 567-0047, Japan*
[2]*Department of Physics, Osaka University, Toyonaka, Osaka 560-0043, Japan*
[3]*Advanced Science Research Center, Japan Atomic Energy Agency, Tokai, Ibaraki 319-1195, Japan*
[4]*Department of Physics, Kyoto University, Kyoto, 606-8502, Japan*
[5]*Instituto de Física Corpuscular, CSIC-Universidad de Valencia, E-46071 Valencia, Spain*
[6]*Institute of Nuclear Research (ATOMKI), H-4001 Debrecen, Post Office Box 51, Hungary*
[7]*National Superconducting Cyclotron Laboratory, Michigan State University, East Lansing, MI 48824-1321, USA*
[8]*Joint Institute for Nuclear Astrophysics, Michigan State University, East Lansing, MI 48824, USA*
[9]*Department of Physics and Astronomy, Michigan State University, East Lansing, MI 48824, USA*
[10]*Institut für Kernphysik, Universität zu Köln, 50937 Köln, Germany*
[11]*Graduate School of Science and Technology, Niigata University, Niigata 950-2181, Japan*
[12]*Department of Physics, Istanbul University, Istanbul 34134, Turkey*
[13]*Institut für Kernphysik, Westfälische Wilhelms-Universität, D-48149 Münster, Germany*

Using the high resolution ^{18}O(^{3}He,t)^{18}F reaction at 0° and at 140 MeV/nucleon, Gamow-Teller (GT) transitions were studied. A high energy-resolution of 31 keV was achieved by applying dispersion matching techniques. The main part of the observed GT transition strength is concentrated in the transition to the ^{18}F ground state (g.s.). The absolute values of the reduced GT transition strengths, B(GT), were derived up to $E_x = 12$ MeV assuming proportionality between the B(GT) values and the reaction cross sections at 0°. The B(GT) value obtained from the β decay of ^{18}F g.s. $\rightarrow$ ^{18}O g.s. was used to determine the proportionality constant. A total B(GT) of 4.06(5) was found and 76(1)% of the strength is concentrated to the g.s. of ^{18}F. The obtained B(GT) values were compared with those from the ^{18}O$(p,n)^{18}$F reaction and the mirror symmetric β^+ decay of ^{18}Ne $\rightarrow$ ^{18}F. The candidates for 1^+ states with isospin $T = 1$ were identified by comparison with the ^{18}O(p,p') data. The results of Shell-Model and QRPA calculations suggest constructive contributions of various configurations to the ^{18}F g.s., suggesting that this state is the *L*ow-energy Super GT (LeSGT) state.

PACS numbers:

I. INTRODUCTION

Gamow-Teller (GT) transitions with $\Delta J^\pi = 1^+$ are mediated by the simple $\sigma\tau$ operator and therefore are characterized by no orbital angular momentum transfer ($\Delta L = 0$) and spin-isospin flip nature ($\Delta S = 1$ and $\Delta T = 1$). GT transitions from a nucleus with Z and N to states in a neighbouring nucleus with $Z \mp 1$ and $N \pm 1$ are called GT$^\pm$ transitions by analogy from the $\beta^\pm$-decay. Thus GT$^\pm$ transitions have the nature of $\Delta T_z = \pm 1$, where T_z is the third component of isospin T and defined by $(N - Z)/2$. The reduced GT transition strength B(GT) is an important physical quantity for our understanding of the nuclear structure [1–3] as well as for the calculation of astrophysical processes [4, 5].

Absolute B(GT) values can be determined directly from β-decay studies. However, these studies are limited by the decay Q-values. On the other hand, charge exchange (CE) reactions, such as (p,n) or (^{3}He,t), performed at 0° and at intermediate incoming energies ($E_{in} > 100$ MeV/nucleon) can be used to map the GT

*hfujita@rcnp.osaka-u.ac.jp
†Present address: Department of Physics and Applied Physics, University of Massachusetts Lowell, Lowell, Massachusetts 01854, USA
‡Present address: Institute for Defense Analyses, Alexandria VA USA, 22311
§Present address: Tokyo Women's Medical University, Shinjuku, Tokyo, 162-8666, Japan
¶Present address: Comisión Chilena de Energía Nuclear, Post Office Box 188-D, Santiago, Chile
**Deceased
††Present address: Institute for Work Design of North Rhine-Westphalia, Radiation Protection Services, 40225 Düsseldorf, Germany
‡‡Present address: CYRIC, Tohoku University, Aramaki, Aoba, Sendai, 980-8578, Japan
§§Present address: RIKEN Nishina Center, Wako, Saitama 351-0198, Japan

strengths over a wider range of excitation energies. For this purpose, one relies upon the approximate proportionality between the reaction cross sections at 0° and the B(GT) values [3, 6, 7].

The pioneering (p,n) reactions performed at 120−200 MeV revealed bump-like resonance structures of GT strength named Gamow-Teller resonance (GTR) in the high excitation energy (E_x) region of 10−15 MeV. They have a width of a few MeV and carry the main part of the observed GT strength. Systematic study of GTRs have been reported for nuclei heavier than $A \sim 50$ [2, 8, 9].

In 1990s, (^{3}He,t) reaction at intermediate energy became available for the study of GT transitions. One-order of magnitude improvement in energy resolution has been achieved [3] in combining a magnetic spectrometer with dispersion matching techniques [10, 11]. Owing to the better resolution, the GTRs were resolved into many discrete excited states (GT states) in the (^{3}He,t) reaction on f- and pf-shell target nuclei ^{54}Fe, ^{58}Ni, and ^{64}Ni [12–14]. In addition, in a recent systematic study on the f-shell $N = Z + 2$ target nuclei ^{42}Ca, ^{46}Ti, ^{50}Cr, and ^{54}Fe, it was found that the distributions of GT strengths are strongly mass dependent [15, 16]. In the ^{54}Fe(^{3}He,t)^{54}Co reaction, the GT strength is mainly concentrated in the GTR region ($E_x = 8-13$ MeV). Moving on to the lighter nuclei ^{50}Cr and ^{46}Ti, less GT strength remained in the GTR region is observed. Finally in the ^{42}Ca(^{3}He,t)^{42}Sc reaction, the GT strength was mostly concentrated in the 1^+_1 state, which was named the *Low-energy Super-GT* (LeSGT) state [15, 16]. Note that the ^{42}Ca nucleus has the ^{40}Ca+2n structure, where the ^{40}Ca behaves as an LS-closed inert core for GT transition. The strong concentration of the GT strength is attributed to the contribution of the isoscalar-type attractive interaction that is active among the particle-particle type configurations on the ^{40}Ca inert core [16–18].

Since ^{18}O nucleus also has the ^{16}O+2n structure, a similar concentration of the GT strength to the 1^+_1 state is expected in the ^{18}O → ^{18}F transition. Using the ^{18}O$(p,n)^{18}$F CE reaction at $E_p = 135$ MeV [19], at 118 MeV [20], and at 494 MeV [21], a strong concentration of the GT transition to the ^{18}F ground state (g.s.) is reported. However, due to the energy resolution of $300 - 500$ keV in the (p,n) reactions, details of the weak GT excitations could not be studied.

In this paper, we will present a study of GT transitions from ^{18}O nucleus via the high resolution ^{18}O(^{3}He,t)^{18}F measurement performed at the Research Center for Nuclear Physics (RCNP), Osaka. Owing to the high energy-resolution realized by the use of the Grand Raiden magnetic spectrometer and application of the dispersion matching techniques [10, 11], not only the strongly excited g.s., but also weakly excited GT states could be studied up to 12 MeV.

II. PROPERTIES OF SPIN-ISOSPIN EXCITATIONS

A. Reduced transition strengths

The reduced GT transition strength B(GT) is defined by

$$B(\mathrm{GT}) = \frac{1}{2}\frac{1}{2J_i+1}\frac{C^2_{\mathrm{GT}}}{2T_f+1}\left|M(\sigma\tau)\right|^2, \tag{1}$$

where C_{GT} and $M(\sigma\tau)$ are the isospin Clebsch-Gordan (CG) coefficient and the doubly reduced $\sigma\tau$ transition matrix element, respectively [3]. In CE reactions at 0° and at intermediate incident energies, the close proportionality between the reaction cross sections and the B(GT) values is given by [3, 6, 7]

$$\frac{d\sigma_{\mathrm{GT}}}{d\Omega} = \hat{\sigma}_{\mathrm{GT}} f_{\mathrm{GT}}(\omega) B(\mathrm{GT}), \tag{2}$$

where $\hat{\sigma}_{\mathrm{GT}}$ is the GT unit cross section at energy transfer $\omega = 0$. The factor $f_{\mathrm{GT}}(\omega)$ gives the dependence of the GT cross section on the energy transfer and thus momentum transfer, which takes value 1 at $\omega = 0$.

In the Fermi transition, a similar proportionality

$$\frac{d\sigma_{\mathrm{F}}}{d\Omega} = \hat{\sigma}_{\mathrm{F}} f_{\mathrm{F}}(\omega) B(\mathrm{F}) \tag{3}$$

is expected.

The R^2 value is defined as the ratio of GT and Fermi unit cross sections [7, 22, 23],

$$R^2 = \frac{\hat{\sigma}_{\mathrm{GT}}}{\hat{\sigma}_{\mathrm{F}}}, \tag{4}$$

which is a measure representing the ratio of strengths of the τ and $\sigma\tau$ terms of the effective interaction at a specific beam energy.

Proton inelastic scattering (IE) performed at small scattering angles, especially at 0° and intermediate energies are also a good tool to study the $\sigma\tau$ response of nuclei [3, 24]. In analogy with the $M1$ transitions via the electromagnetic interaction, we call $\Delta J^\pi = 1^+$ transitions caused by the (p,p') reaction as $M1_\sigma$ transitions [3].

Neglecting the contributions from the σ and other minor non-$\sigma\tau$ terms, a proportionality similar to Eq. (2) is expected in the (p,p') reaction [25–27],

$$\frac{d\sigma_{M1}}{d\Omega} \approx \hat{\sigma}_{M1} f_{M1}(\omega) B(M1_\sigma). \tag{5}$$

We define $B(M1_\sigma)$ [3], the reduced transition strength assuming pure $\sigma\tau$ interaction, as

$$B(M1_\sigma) = \frac{1}{2}\frac{1}{2J_i+1}\frac{C^2_{M1}}{2T_f+1}\left|M(\sigma\tau)\right|^2, \tag{6}$$

where C_{M1} is the isospin CG coefficient for the transitions to $M1$ states. Assuming isospin symmetry and no contribution of meson exchange current (MEC) [28, 29], identical $M(\sigma\tau)$ values are expected for analogous transitions to GT and $M1$ states.

B. Isospin symmetry in $A = 18$ system

In Fig. 1, the ^{18}O $\rightarrow$ ^{18}F GT transitions and the analogous transitions are summarized with the corresponding isospin CG coefficients. The ^{18}O nucleus has $T_z = (N - Z)/2 = +1$ and initial isospin $T_0 = 1$. By the GT$^-$ transitions from the ^{18}O nucleus, therefore, GT states with $T = 0$, 1, and 2 in ^{18}F ($T_z = 0$) nucleus are nominally expected, as shown in Fig. 1. On the other hand, in the IE scattering such as (p, p'), $M1$ states with $T = 1$ and 2 in ^{18}O are expected. Because $T_z = +1$ in ^{18}O, a final isospin of $T = 0$ is forbidden.

In the naive Shell-Model picture, the g.s. of ^{18}O is described by the LS-closed ^{16}O inert core having $T = 0$ plus two valence neutrons occupying the $d_{5/2}$ orbit. This picture suggests that the final GT states in ^{18}F have a proton (π) and a neutron (ν) with configurations of $(\pi d_{5/2}, \nu d_{5/2})$ and $(\pi d_{3/2}, \nu d_{5/2})$ and the total isospin is determined by these two valence nucleons. Since $T = 2$ cannot be formed by two nucleons, the GT states with $T = 2$ cannot be excited in ^{18}F without breaking the ^{16}O inert core. By the same reason, the $M1$ states with $T = 2$ are not allowed in ^{18}O nucleus. The $T = 2$ states, therefore, are shown with dashed lines in Fig. 1.

Assuming isospin symmetry, the identical values are expected for the matrix elements $M(\sigma\tau)$ in Eqs. (1) and (6) for the analogous GT and $M1_\sigma$ transitions. Since the isospin CG coefficients $C_{\rm GT}$ and C_{M1} for the GT and $M1_\sigma$ transitions to the $T = 1$ states are the same (see Fig. 1), it is expected that the corresponding B(GT) and $B(M1_\sigma)$ values are also identical.

It should be noted that, existence of large components of high-momentum neutrons in the ^{16}O g.s. due to the tensor interaction was suggested via the ^{16}O$(p, d)^{15}$O reaction recently [30]. This result suggests that the inert ^{16}O core is not closed and therefore the GT and $M1$ states with $T = 2$ can exist. However, even if they exist, the IAS of ^{18}N g.s. having $T = 2$ is expected at $E_x \sim 16$ MeV in ^{18}O, which corresponds to 17 MeV in ^{18}F. This energy region is, however, out of observable region of the present data.

III. EXPERIMENT

The ^{18}O(^{3}He,t)^{18}F experiment was performed at the Research Center for Nuclear Physics (RCNP), Osaka University. The lateral and angular dispersion matching techniques [10] were applied in order to realize high energy-resolution and good scattering angle resolution in the horizontal direction, respectively. A 140 MeV/nucleon ^{3}He^{2+} beam of $\sim$5 enA from the RCNP ring cyclotron [31] was transported onto the target by using the WS course beamline [32]. A diagnostic method of dispersion matching and focusing conditions, the *faint beam method* [11], was applied, in order to realize matching conditions.

The enriched ^{18}O gas was filled in a gas cell target system [33] with aramid foil windows. For the background subtraction, the measurement with an aramid foil target was performed. Scattered tritons were momentum analyzed by the Grand Raiden magnetic spectrometer [34] located at 0°. The ^{3}He^{2+} beam was stopped in a Faraday cup placed inside the first dipole magnet of Grand Raiden.

The tritons were detected by the two multiwire drift chambers (MWDCs) [35] placed along the focal plane with an angle of 45° relative to the central ray of the spectrometer. Each MWDC consists of two anode wire planes, with one set of sense wires stretched vertically (X) and another set of wires tilted at an angle of 48.2° (U) with respect to the vertical direction. By combining the X and U position information, vertical position (Y) in the focal plane was also obtained. Incident angles of the particles were obtained by the X and Y information from the two MWDCs. Two plastic scintillators downstream of the MWDCs were used for the particle identification and the generation of timing signals.

In order to achieve good scattering angle resolution in the vertical direction, the over-focus mode [36] of Grand Raiden was applied. In combination with the angular dispersion matching technique [10], precise measurements of the scattering angles in both horizontal and vertical directions were realized. The precise 0° scattering angle was determined from the incident angle of singly charged ^{3}He$^+$ particles in the focal plane that are produced by atomic-electron capture processes in the target. Defocusing effects in the detector plane due to the kinematic recoil and aberration of the magnetic field were corrected by software.

IV. DATA ANALYSIS

A. Peak fitting and E_x calibration

The ^{18}O(^{3}He,t)^{18}F spectra with different vertical scales are given in Fig. 2, where the events within the scattering angles of $0.0° - 0.5°$ are selected. As a result of the software corrections, an energy resolution of 31 keV ($\Delta E/E = 7.4 \times 10^{-5}$) was achieved. The overview is given in Fig. 2 (a), while the vertical scales are expanded by a factor of eight and one hundred in Fig. 2 (b) and (c), respectively. Before the peak fitting analysis, the background (BG) events originated from the Aramid foil windows of the gas cell and nitrogen in the contaminated air were subtracted. The spectrum after the BG subtraction is shown in Fig. 2 (d).

Positions and counts of the peaks were obtained from the peak fitting analysis [37] using the peak shape of the strongest and isolated ^{18}F g.s. as a reference. The shapes of the states having decay widths Γ were reproduced by combining the reference peak shape and the width represented by a Lorentzian function. Above the proton separation energy S_p of 5.6 MeV, a continuum caused by the

quasi-free scattering (QFS) [38] is expected. Amount of the QFS was estimated as a smoothly increasing function of excitation energy by connecting valleys of the spectra above the proton separation energy (see Fig. 4).

The relationship between the peak positions and the outgoing triton momenta were determined by the known states in ^{12,13}N and ^{16,18}F observed in the data using a polyethylene terephthalate ($C_{10}H_8O_4$) film as a target. From the obtained relationship, the excitation energies of states in ^{18}F were reconstructed. Due to the large difference between the Q-values for ^{18}O(^{3}He,t)^{18}F and ^{12}C(^{3}He,t)^{12}N reactions (-1.67 MeV and -17.36 MeV respectively), excitation energies of states in ^{18}F can be determined by interpolation up to 18 MeV.

In Table I, the E_x values obtained in the present analysis are compared with the evaluated values [39]. The reconstructed excitation energies in ^{18}F are in agreement with the evaluated values within 1 keV accuracies up to 5.6 MeV. Above this energy, the differences between the evaluated and reconstructed values are typically 5 keV. It should be noted that the uncertainties of the evaluated values are less than 0.3 keV below $E_x = 5.6$ MeV, whereas above this excitation energy their uncertainties are about $1 - 3$ keV.

B. $\Delta L = 0$ identification

It is known that the angular distributions for the GT transitions, having the orbital angular momentum transfer $\Delta L = 0$ nature, show maximum cross section at 0° and a characteristic rapid decrease at larger scattering angles. On the other hand, such angular distribution is not expected for the $\Delta L \geq 1$ transitions. In order to identify GT states, the angular distributions of the observed states were examined.

We define the "ratio of ratio" of counts, Rr, as follows. First, the counts of states in the spectra for the scattering angles of $0.0° - 0.5°$, $0.5° - 0.8°$, $0.8° - 1.2°$, $1.2° - 1.6°$, and $1.6° - 2.0°$, which will be denoted with a subscript $j = 0-4$, were normalized by the counts in the $0.0° - 0.5°$ (i.e. $j = 0$) spectrum. These ratios for each state were further normalized by the corresponding ratios of the ^{18}F g.s., which is the strongest GT state. Therefore, the Rr_j ratios are defined by

$$Rr_j = \frac{N_j}{N_0} \Bigg/ \frac{N_j^{g.s.}}{N_0^{g.s.}} , \qquad (7)$$

where N_j is the count for each state in the jth spectrum and $N_j^{g.s.}$ is that for the ground state. All the states, therefore, take the ratio $Rr_0 = 1$ by definition. For the states having the $\Delta L = 0$ nature, $Rr_{1-4} \sim 1$ are expected due to the similarity of angular distributions. On the other hand, for the states with $\Delta L \geq 1$ nature, Rr_{1-4} values would be larger than unity because rapidly decreasing angular distribution is not expected. It should be noted that, expected Rr value changes slightly as a function of E_x mainly due to the kinematic effect. By the distorted wave Born approximation reaction calculation for the GT transition, difference of the Rr values at $E_x = 0$ and 15 MeV is estimated to be less than 5 %.

The obtained Rr_4 ratios for the states below 6.5 MeV are summarized in Table I. In this region, the J^π values of most of the observed states are known and the 1^+ and 0^+ states show $Rr_4 \sim 1$ as expected from their $\Delta L = 0$ nature. On the other hand, the 2^+ states at 3.062 MeV and 3.839 MeV, and the 2^- state at 5.786 MeV show larger Rr_4 values as expected from their $\Delta L \geq 1$ nature. It should be noted, however, the 3^+ state at 0.937 MeV shows Rr_4 value similar to those of the 1^+ states, which was discussed in detail in Ref. [16]. As examples, angular distributions and the obtained Rr_{0-4} values for the low-lying states are shown in Fig. 3. The angular distribution of the ^{18}F g.s., which was used as the normalization standard of the Rr_j values, is also shown.

For the weakly excited peak at 5.60 MeV, $Rr_4 = 1.9$ was obtained. Since this peak can be a doublet of the 1^+ and 1^- states at 5.603 MeV and 5.605 MeV, respectively, the large Rr_4 can be attributed to the contribution from the 1^- state. The peak at 6.10 MeV, having $Rr_4 > 5$, can also be a mixture of the 1^+ and 4^- states at 6.108 MeV and 6.096 MeV. In both cases, even if the obtained counts in the $0.0° - 0.5°$ spectrum are purely from the 1^+ states, the estimated B(GT) values for these peaks are less than our detection limit of $B(\mathrm{GT}) = 0.01$.

In Fig. 4 (a), (b), and (c), the ^{18}O(^{3}He,t) spectra from 6.5 to 12.5 MeV are shown for the scattering angles $0.0° - 0.5°$, $0.8° - 1.2°$, and $1.6° - 2.0°$, where the events from the contaminating nuclei are subtracted. The deteriorated parts in the spectra due to the subtraction are hatched. The estimated QFS continuum is shown by dashed lines. Since the counts in Fig. 4 are normalized by the corresponding solid angles, relative peak heights of the states roughly represent the angular distributions.

In Table II, Rr_4 ratios, excitation energies, and widths of peaks (Γ) are summarized for the states above 6.5 MeV. Candidates for the corresponding states evaluated in Ref. [39] are also shown. Ambiguities of the width Γ was estimated from the results of the peak fitting analysis using the spectra for different scattering angles. For most of the states, more-or-less good agreements of widths were found.

A peak observed at 7.42 MeV becomes weaker at larger scattering angles, as can be seen in Fig. 4 (a)−(c). Although this state shows relatively large Rr_4 value of 2.3, we tentatively give $\Delta L = 0$ assignment for this state since the Rr_{1-3} values of this state are within $1.0 - 1.5$. It should be noted that there is a corresponding 1^+ state at 7.406 MeV [39]. Except for this state, all of the observed states between 6.5 MeV and 8.5 MeV become stronger at larger scattering angles (see Fig. 4), suggesting their $\Delta L \geq 1$ nature.

Above 9 MeV, most of the states show Rr_{1-3} of 0.9−1.3, however, Rr_4 values are $1.4 - 1.5$ except for the 9.65 MeV state with $Rr_4 = 0.75$. As shown in Fig. 2

(c)−(d) and Fig. 4, this region suffers from the large BG events and the QFS continuum, which may introduce large ambiguities to the Rr_{1-4} values. Therefore, we give tantative $\Delta L = 0$ assignments for these states as summarized in Table II.

C. Estimation of the $f_{\rm GT}(\omega)$ term

The energy transfer ω dependence of the $f_{\rm GT}(\omega)$ value in Eq. (2) was estimated from the reaction cross sections calculated by a series of distorted wave Born approximation (DWBA) codes, WSAW, FOLD, and DWHI [40]. Optical potential parameters for the ^{18}O+^{3}He channel were estimated by interpolating the values derived for ^{16}O and ^{28}Si [41–44]. For the outgoing ^{18}F+triton channel, the well depths were multiplied by a factor of 0.85 without changing the geometrical parameters following the arguments given in Ref. [45]. In these calculations, pure $\sigma\tau$-type interaction was assumed.

The $f_{\rm GT}(\omega)$ estimation was performed as follows. First, averaged values of the cross sections at 0° assuming $\pi d_{5/2} \rightarrow \nu d_{5/2}$ and $\pi d_{5/2} \rightarrow \nu d_{3/2}$ transitions were calculated as a function of energy transfer ω. The $f_{\rm GT}(\omega)$ values were then estimated by normalizing the averaged cross sections to 1 at $\omega = 0$. The estimated $f_{\rm GT}(\omega)$ value gradually decreases with increasing excitation energy and the amount of decrease from $E_x = 0$ to 10 MeV was about 10%. Contributions of the $\Delta L = 2$ component in the DWBA calculations at 0° was less than 0.1% in both configurations. For the Fermi transition, the $f_{\rm F}(\omega)$ term was estimated in a similar way.

D. Derivation of the B(GT) values and the R^2 ratio

In order to derive the absolute B(GT) values using Eq. (2), a standard B(GT) value is needed. It was determined from the ^{18}F β^+ decay, which connects the ^{18}F g.s. (1^+) and the ^{18}O g.s. (0^+) in opposite direction to the ^{18}O(^{3}He,t)^{18}F reaction (see Fig. 1). From the half-life and the Q-value given in Ref. [39], the B(GT) value of 1.031(5) was obtained. Taking the factor of three for the reversed transition into account, a B(GT) value of 3.092(16) was obtained for the ^{18}O g.s. $\rightarrow$ ^{18}F g.s. GT transition.

The derived B(GT) values using this standard B(GT) value are summarized in Table III. We estimate that reasonably precise B(GT) values are deduced for the transitions with derived values larger than 0.01. Except for the ^{18}F g.s., no strong GT transition was found. The total GT strength is 4.06(5) and 76(1)% of that is concentrated in the transition to the ground state. Assuming no GT$^+$ transition, it is 68% of the Ikeda GT sum rule value of $3(N-Z) = 6$.

Ratio of the GT and Fermi unit cross sections, i.e., the R^2 value [7, 22, 23], was deduced from the present data. From the observed strengths of the ^{18}F g.s. and the IAS at 1.043 MeV in the $0.0° - 0.5°$ spectrum, $R^2 = 6.45(6)$ was obtained. For comparison, the R^2 value from the ^{42}Ca(^{3}He,t)^{42}Sc data [16] was also deduced from the 1^+_1 state at 0.611 MeV and the IAS (g.s.). As a result, the identical R^2 value with larger ambiguity of 6.45(18) was obtained. It should be noted that, from the GT and Fermi unit cross sections given in Ref. [46] as the functions of A, the R^2 value of 4.94 and 6.99 are suggested for $A = 18$ and 42, respectively. Numerical parameters are summarized in Table IV.

V. DISCUSSION

A. Comparison with the available data

In Table III, the present B(GT) values derived from the present ^{18}O(^{3}He,t)^{18}F data up to $E_x = 12$ MeV are shown. The B(GT) values from the ^{18}Ne β-decay [39, 47], the ^{18}O(p,n) reactions [19–21], and the $B(M1_\sigma)$ values from the ^{18}O(p,p') scattering data [26] are also shown. In Fig. 5, these B(GT) and $B(M1_\sigma)$ values are shown together. The E_x value of the ^{18}O(p,p') result is shifted by 1.1 MeV so that the analog states are expected to be aligned.

Between the B(GT) values from the present study and those from the mirror symmetric ^{18}Ne $\rightarrow$ ^{18}F β-decay (see Fig. 1), isospin symmetry was examined. The B(GT) and B(F) values from the ^{18}Ne β-decay were deduced by combining the recently published half-life [47] with the branching ratios and the decay Q-value given in Ref. [39]. For the transition to the ^{18}F g.s., the ^{18}Ne β-decay gives a B(GT) value of 3.123(24), which is consistent with the present standard value of 3.092(16) within the uncertainties. For the Fermi transition, B(F) of 2.11(6) is also reasonably consistent with the expected value of $N - Z = 2$ suggesting consistency of the data. On the other hand, the B(GT) value of 0.131(5) for the 1^+_2 state at 1.701 MeV is smaller than the present value of 0.170(2).

The B(GT) values from the ^{18}O(p,n) data at $E_p =$ 135 MeV [19], 118 MeV [20], and at 494 MeV [21] in Table III are renormalized by using the present standard value of 3.092(16). Ambiguities of the B(GT) values at 135 MeV were estimated from the relative uncertainties of the cross sections of 5% as given in Ref. [19]. For the 1^+_2 state at 1.701 MeV, the present value of 0.170(2) is $10 - 20$% smaller than those from the (p,n) data at 135 MeV and at 118 MeV. For the states at 3.725, 4.361, and 6.256 MeV, consistent B(GT) values within the uncertainties are found.

Above 9 MeV, E_x values for the GT states are reasonably consistent with the (p,n) measurements [19, 20] as shown in Table III. Assuming the peaks at 9.65 MeV and 9.92 MeV are observed as one peak at 9.9 MeV in the (p,n) measurements, the B(GT) values from the present data and the $E_p = 118$ MeV data [20] agree with each

other. The B(GT) value for the 11.1 MeV state from the E_p = 118 MeV data is also consistent with the present data for the 10.9 MeV state.

As the total B(GT) strengths, 3.80(3), 4.10(5), and 4.2(5) were obtained from the (p,n) data at E_p = 135 MeV [19], 118 MeV [20], and 494 MeV [21], respectively. These values are consistent reasonably with the present value of 4.06(5).

As discussed above, it is expected that analogous 1^+ states with isospin $T = 1$ are observed commonly in the present ^{18}O(^{3}He,t) and ^{18}O(p,p') data. From Eqs. (1) and (6) and isospin CG coefficients for the $T = 1$ states (see Fig. 1), B(GT) and $B(M1_\sigma)$ are expected to be identical for analogous GT and $M1$ states. The $B(M1_\sigma)$ values shown in Table III were converted from the $B(\sigma)$ values from the ^{18}O(p,p') data [26] at 201 MeV, following the descriptions given in Refs. [3, 48], neglecting contributions of non-$\sigma\tau$-type transitions.

For the state at 9.92 MeV, B(GT) value of 0.07(2) was obtained from the present data. Since the IAS in ^{18}F is at 1.043 MeV, the analog state is expected at around 8.9 MeV in ^{18}O. At the corresponding energy of 8.82 MeV, 1^+ state with a consistent $B(M1_\sigma)$ value of 0.07(1) was found from the ^{18}O(p,p') data [26]. This fact suggests that these states are in analogous relationship and thus have isospin $T = 1$.

From the present data, the GT states were found at 10.9 and 11.8 MeV. As discussed above, the corresponding 1^+ states are also reported from the (p,n) data [19, 20]. On the other hand, from the (p,p') data [26], a broad bump structure is reported at E_x = 10.10 MeV with the $B(M1_\sigma)$ value of 0.31(4). Since this value agrees with sum of the strengths for the states at 10.9 and 11.8 MeV, 0.26(8), within the ambiguities, we assign isospin $T = 1$ for both of the 10.9 and 11.8 MeV states. The B(GT) and $B(M1_\sigma)$ values discussed here are summarized in Table III and Fig. 5.

In the (p,p') data [26], another bump structure was observed between 12.4−15 MeV. Since no corresponding strength is reported from the (p,n) data, this structure can be the giant dipole resonance (GDR), which is excited via the electromagnetic interaction.

B. Low-energy Super Gamow-Teller (LeSGT) state

As is given in Table III, the B(GT) value of 3.092(16) is obtained for the transition to the ^{18}F g.s. (1^+_1). This value corresponds to 76(1)% of the total strength up to 12 MeV. A similar concentration of the GT strength to the 1^+_1 state is reported in the ^{42}Ca(^{3}He,t)^{42}Sc reaction [15, 16]. A large B(GT) value of 2.17(5), which corresponds to about 80% of the observed strength, was concentrated in the transition to the 1^+_1 state. Note that, the $A = 18$ and $A = 42$ systems are expected to have the same structure in the sense that they consist of LS-closed core and two valence nucleons.

In the Shell-Model (SM) calculation using the GXPF1J interaction for the GT transition from the ^{42}Ca 0^+ g.s. to the ^{42}Sc 1^+_1 state, it was shown that several f- and p-shell configurations make an in-phase contributions [15, 16]. Similarly, QRPA calculations also show that this state has a collective nature, which is originated from the isoscalar attractive interaction among the particle-particle type configurations of the valence nucleons [15–17]. As a result, a large part of the available single-particle transition strengths are concentrated to the 1^+_1 GT state in ^{42}Sc. Because of the collective nature of this state, the 1^+_1 state at 0.611 MeV in ^{42}Sc was named *L*ow-energy Super Gamow-Teller (LeSGT) state [15, 16, 18, 49].

Let us discuss the properties of the ^{18}F g.s. (1^+_1) from an empirical view point. In Ref [20], the GT strengths observed in the ^{17}O$(p,n)^{17}$F reaction are presented. Starting from the ^{17}O g.s. with $J^\pi = 5/2^+$, two GT transitions to the ^{17}F g.s. $(5/2^+_1)$ and the state at 5.00 MeV $(3/2^+_1)$ with B(GT) = 1.062 and 0.57 are reported. They would correspond to the $\nu d_{5/2} \to \pi d_{5/2}$ and $\nu d_{5/2} \to \pi d_{3/2}$ transitions on top of the inert ^{16}O core, respectively. Here, we notice that twice of the sum of the B(GT) values observed in the ^{17}O$(p,n)^{17}$F reaction agrees well with the present B(GT) value for the ^{18}F g.s., i.e., 3.092(16). This fact suggests that the contributions of the $\nu d_{5/2} \to \pi d_{5/2}$ and $\nu d_{5/2} \to \pi d_{3/2}$ transitions make in-phase contributions in the transition to the ^{18}F g.s. and therefore this state has the nature of the LeSGT state.

This picture also suggests the existence of the state, in which the $\nu d_{5/2} \to \pi d_{5/2}$ and $\nu d_{5/2} \to \pi d_{3/2}$ contributions cancell each other. Such state can be called as "anti-LeSGT" state [49]. In the SM calculation for the ^{42}Ca $\to$ ^{42}Sc case [16], strong cancellation between the $\nu f_{7/2} \to \pi f_{7/2}$ and $\nu f_{7/2} \to \pi f_{5/2}$ components was found in the transition to the 1^+_2 state, suggesting that this state has the nature of the anti-LeSGT state. We expect the anti-LeSGT state exists also in ^{18}F, with similar destructive contribution between the $\nu d_{5/2} \to \pi d_{5/2}$ and $\nu d_{5/2} \to \pi d_{3/2}$ components.

C. Shell-Model calculations

The Shell-Model (SM) calculation for the GT transition of the ^{42}Ca $\to$ ^{42}Sc case showed that f- and p-shell configurations make an constructive contribution to the 1^+_1, LeSGT state [15, 16]. In order to study whether similar contributions exist also in the $A = 18$ system or not, SM calculations were performed for the ^{18}O $\to$ ^{18}F case.

In Fig. 6, the B(GT) strength distributions are shown from (a) the present ^{18}O(^{3}He,t) data, those from the SM calculations using the interactions (b) the USDA [50], (c) the USDB [50], and (d) the modified-PSDWBT [51]. The GT quenching factor is not included.

Up to 8 MeV, the observed fragmentation of the GT strength distribution [Fig. 6 (a)] was well reproduced by the modified-PSDWBT calculation [Fig. 6 (d)]. This

would be because the modified-PSDWBT interaction can describe multi-particle multi-hole states within the *p*-*sd* model space [51]. Above 8 MeV, higher level density was suggested by the calculation, however, the level density in this region can not be derived from the present data because of the decay widths of the observed states (see Fig. 4).

Concentration of the GT strength to the 1^+_1 state was reproduced in all of the SM calculations. Our experiment shows that, 74(1)% of the total strength is concentrated in the ^{18}F g.s. (1^+_1). On the other hand, in the SM calculations using USDA, USDB, and modified-PSDWBT interactions, 86%, 87%, and 78% of the total strength, respectively, are concentrated in the 1^+_1 state.

In order to understand the transitions to the low-lying states, we examined the SM calculations in the simple *sd* model space using the USDA and USDB interactions. In Fig 7, the GT matrix elements for different components from the calculations are illustrated for the 1^+_1, 1^+_2, and 1^+_3 states. Square of the summed value of the GT matrix elements corresponds to the B(GT). As expected from a naive SM picture, the components starting from the $d_{5/2}$ orbit make large contributions and those from the $d_{3/2}$ are small. Relatively large contributions are found from the $2s_{1/2}$ orbit.

As can be seen in Fig 7, in the transition to the 1^+_1 state, the constructive contributions from the $\nu d_{5/2} \rightarrow \pi d_{5/2}$, $\nu d_{5/2} \rightarrow \pi d_{3/2}$, and $\nu 2s_{1/2} \rightarrow \pi 2s_{1/2}$ components are realized. These results strongly support that this state has characteristics quite similar to the 1^+_1 state in ^{42}Sc [15, 16].

In the transition to the 1^+_3 state, both USDA and USDB calculations show strong cancellation between the $\nu d_{5/2} \rightarrow \pi d_{5/2}$ and $\nu d_{5/2} \rightarrow \pi d_{3/2}$ components, which makes B(GT) values small (see Fig. 7). Note that the absolute values of the GT matrix elements are similar to those in the 1^+_1 state. These results suggest that the 1^+_3 state have the characteristics of an anti-LeSGT state. The 1^+_3 state appears at 6.6 and 7.4 MeV in the USDA and USDB results, respectively. In the present data, a few weakly excited GT states were found in this region, however, empirical identification of the anti-LeSGT state is not clear.

As we see in Fig. 7, strong cancellation between the $\nu d_{5/2} \rightarrow \pi d_{5/2}$ and $\nu 2s_{1/2} \rightarrow \pi 2s_{1/2}$ components is found for the 1^+_2 state in both of the USDA and the USDB results. This characteristic cancellation may suggest that the 1^+_2 state also has anti-LeSGT nature, like the 1^+_3 state.

As shown in Fig. 6 (b)-(d), all the SM calculations show characteristic concentration of $T = 1$ GT strength around $E_x \sim 12$ MeV. However, as described above and shown in Fig. 6 (a), we suggest that the $T = 1$ GT strength is fragmented in the $E_x = 10 - 12$ MeV region.

D. QRPA calculation

For the ^{42}Ca $\rightarrow$ ^{42}Sc case, the strong concentration of the GT strength to the 1^+_1 state was explained by the competition of isoscalar (IS) and isovector (IV) pairing interactions [15–17]. Following the $A = 42$ case, let us discuss here the GT strength distribution in the ^{18}O $\rightarrow$ ^{18}F case from the similar point of view. For this purpose, a self-consistent Hartree-Fock-Bogoliubov (HFB) plus quasiparticle-random-phase approximation (QRPA) calculation [52] using the Skyrme interaction SGII [53] was performed.

First, HFB and QRPA standard calculations including the IV, $T = 1$, pairing interaction were performed. Here, the surface-type density-dependent contact interaction with a strength $V_0 = -490$ MeV fm^3 was employed. Then, we introduced the IS interaction between proton particle and neutron particle (πp-νp), i.e., the $T = 0$ pairing interaction in the QRPA part of the calculation. Its strength is expressed by the factor f defined by the ratio of the strengths of the IS pairing interaction to that of the IV pairing interaction (for details, see Ref. [17]).

The obtained GT strength distribution varying the factor f is shown in Fig. 8, where the excitation energy E_x is given with respect to the g.s. of the ^{18}O nucleus. A width of 0.5 MeV was introduced to smear the strength distributions. We see that the GT strength is mainly divided into the lower-energy (LE) and higher-energy (HE) peaks. The origin of these states can be qualitatively explained by the involvement of the two-quasiparticle (2qp) configurations of $\pi d_{5/2} \otimes \nu d_{5/2}$ and $\pi d_{3/2} \otimes \nu d_{5/2}$, which are formed by the $\nu d_{5/2} \rightarrow \pi d_{5/2}$ and $\nu d_{5/2} \rightarrow \pi d_{3/2}$ transitions, respectively. To make discussion comparable with the other part, components of the transitions will be described in the latter form.

As shown in Fig. 8, when $f = 0$, i.e., without the IS pairing interaction, main part of the GT strength is in the HE peak situated at 13.5 MeV. The LE peak at 6.8 MeV with smaller GT strength is mainly excited by a $\nu d_{5/2} \rightarrow \pi d_{5/2}$ transition. With the increase in f, the peaks move to lower energy. At the same time, the GT strength of the HE peak becomes weaker and the LE peak acquires more strength (see Fig. 8). Eventually, in the case of $f = 1.3$, the LE peak appears 1 MeV below the IAS, being consistent with the E_x values of the 1^+_1 (g.s.) and the IAS (1.043 MeV).

In Table V, the obtained B(GT) values and the reduced GT matrix elements for different components with $f = 1.3$ are summarized. Transition to the LE peak is mainly contributed from the $\nu d_{5/2} \rightarrow \pi d_{5/2}$ component. Furthermore, the $\nu d_{5/2} \rightarrow \pi d_{3/2}$ and $\nu d_{3/2} \rightarrow \pi d_{5/2}$ components make constructive contributions to the excitation of the LE peak. It should be noted that, this result is reasonably consistent with the SM calculation. Thus, because of the strong collectivity suggested from both of the SM and QRPA calculations, we conclude that the 1^+_1 state in ^{18}F is LeSGT state. The present QRPA calculation suggests this collectivity is generated by the

IS πp-νp residual interaction.

With $f = 1.3$, we see a tiny peak at 7.9 MeV (see Fig. 8). As shown in Table V, the QRPA calculation also suggests that this state is generated by the destructive contribution mainly between the $\nu d_{5/2} \rightarrow \pi d_{5/2}$ and the $\nu d_{5/2} \rightarrow \pi d_{3/2}$ components, suggesting the existence of the anti-LeSGT state.

The HE peak is predominantly constructed by the remaining $\nu d_{5/2} \rightarrow \pi d_{3/2}$ component that was not absorbed in the LE peak. Since this state locates ~ 7 MeV higher than the IAS, the corresponding E_x value in ^{18}F is about 8 MeV. This state may correspond to the excited states around $9 - 12$ MeV [see Fig. 6 (a)].

VI. SUMMARY AND CONCLUSION

We have performed high resolution ^{18}O(^{3}He,t)^{18}F measurements at 140 MeV/nucleon and at an angle around 0°. Owing to the high energy-resolutions of 31 keV, most of the excited states in ^{18}F are well separated. For the transition to the g.s. of ^{18}F (1^+_1), a strong concentration of the Gamow-Teller transition strength was found. By using the standard B(GT) value of 3.092(16) obtained from the β-decay of ^{18}F, B(GT) values for the observed 1^+ states were determined up to 12 MeV.

A total B(GT) of 4.06(5) was found and 76(1)% of the strength is concentrated to the ground state. The obtained B(GT) values were reasonably consistent with the available (p, n), (p, p'), and β-decay data.

The SM calculations applying the USDA and USDB interactions suggest in-phase contribution of the $\nu d_{5/2} \rightarrow \pi d_{5/2}$ and $\nu d_{5/2} \rightarrow \pi d_{3/2}$ components in the GT transition to the ^{18}F g.s. (1^+_1) and thus the B(GT) value becomes remarkably large. The mechanism causing the large B(GT) value is similar to the one found for the 1^+_1 state in ^{42}Sc [15, 16].

The QRPA calculations were performed in order to investigate the roles of the effective IS paring interaction in the GT transitions. The results of the calculations suggested the effective IS interaction causes the concentration of the GT strength to the 1^+_1 state. By increasing the strength of the IS interaction, the energy of the 1^+_1 state became lower and the GT strength was more concentrated. The constructive contribution of the two major configurations, i.e., $\nu d_{5/2} \rightarrow \pi d_{5/2}$ and $\nu d_{5/2} \rightarrow \pi d_{3/2}$ is consistent with the SM calculations. Therefore we conclude that the 1^+_1 state in ^{18}F is the LeSGT state.

The SM and QRPA calculations also suggested existence of the anti-LeSGT state, in which the GT strength is weak and the contributions of two major transitions are cancelling each other. In the present ^{18}O(^{3}He,t)^{18}F data, a few candidates were found. However, it was not possible to identify the anti-LeSGT state specifically.

Acknowledgments

The (^{3}He,t) experiment was performed at RCNP, Osaka University, under Experimental Program No. E307. We thank all the staffs of the accelerator group at RCNP for providing a high quality beam. H.F. and Y.F. also acknowledges the support of MEXT, Japan under Grants No. 18540270, No. 22540310, and No. 15K05104. Y.F. and B.R. are grateful for the support of the Japan-Spain collaboration program by JSPS and CSIC; A.A., E.E.A., and B.R. are thankful for the support of the Spanish Ministerio de Economa y Competitividad under Grants No. FPA2005-03993, No. FPA2008-06419-C02-01, No. FPA2011-24553, No. FPA2014-52823-C2-1-P, FPA2017-83946-C2-1-P, and the program Severo Ochoa (SEV-2014-0398). G.S. acknowledges the support of TUBITAK, Turkey under Research Scholarship No. BIDEB 2214. J.M.D., C.J.G., R.M., G.P., and R.G.T.Z. are grateful for the support of the US NSF under Grants No. PHY-0606007 and No. PHY-0822648 (JINA). M.C., J.G. and A.K. acknowledge the support of the NKFI OTKA Foundation, Hungary, under Grant No. K124810. This work was in part supported by the RIKEN-CNS joint research project on large-scale nuclear-structure calculations. K.Y. acknowledges the support of the JSPS KAKENHI (Grant Nos. JP16K17687, JP18H04569, JP19K03824, and JP19K03872), and the JSPS-NSFC Bilateral Program for Joint Research Project on Nuclear mass and life for unraveling mysteries of the r-process. The QRPA calculations were performed on CRAY XC40 at the Yukawa Institute for Theoretical Physics, Kyoto University, and on COMA (PACS-IX) at the Center for Computational Sciences, University of Tsukuba.

[1] F. Osterfeld, Rev. Mod. Phys. 64 (1992) 491, and references therein.
[2] J. Rapaport, E. Sugarbaker, Ann. Rev. Nucl. Part. Sci. 44 (1994) 109.
[3] Y. Fujita, B. Rubio, W. Gelletly, Prog. Part. Nucl. Phys. 66 (2011) 549, and references therein.
[4] G. M. Fuller, W. A. Fowler, M. J. Newman, Astrophys. J. 252 (1982) 715.
[5] K. Langanke, G. Martínez-Pinedo, Rev. Mod. Phys. 75 (2003) 819.
[6] C. D. Goodman, C. A. Goulding, M. B. Greenfield, J. Rapaport, D. E. Bainum, C. C. Foster, W. G. Love, F. Petrovich, Phys. Rev. Lett. 44 (1980) 1755.
[7] T. N. Taddeucci, C. A. Goulding, T. A. Carey, R. C. Byrd, C. D. Goodman, C. Gaarde, J. Larsen, D. J. Horen, J. Rapaport, E. Sugarbaker, Nucl. Phys. A 469 (1987) 125, and references therein.
[8] M. N. Harakeh, A. van der Woude, Giant Resonances, Vol. 24 of Oxford Studies in Nuclear Physics, Oxford University Press, 2001, and references therein.

[9] C. Gaarde, Nucl. Phys. A 396 (1983) 127c.
[10] Y. Fujita, K. Hatanaka, G. P. A. Berg, K. Hosono, N. Matsuoka, S. Morinobu, T. Noro, M. Sato, K. Tamura, H. Ueno, Nucl. Instr. and Meth. Phys. Res. B 126 (1997) 274.
[11] H. Fujita, Y. Fujita, G. P. A. Berg, A. D. Bacher, C. C. Foster, K. Hara, K. Hatanaka, T. Kawabata, T. Noro, H. Sakaguchi, Y. Shimbara, T. Shinada, E. J. Stephenson, H. Ueno, M. Yosoi, Nucl. Instr. and Meth. Phys. Res. A 484 (2002) 17.
[12] T. Adachi, et al., Phys. Rev. C 85 (2012) 024308.
[13] H. Fujita, et al., Phys. Rev. C 75 (2007) 034310.
[14] L. Popescu, et al., Phys. Rev. C 79 (2009) 064312.
[15] Y. Fujita, et al., Phys. Rev. Lett. 112 (2014) 112502.
[16] Y. Fujita, et al., Phys. Rev. C 91 (2015) 064316.
[17] C. L. Bai, H. Sagawa, G. Colò, Y. Fujita, H. Q. Zhang, X. Z. Zhang, F. R. Xu, Phys. Rev. C 90 (2014) 054335.
[18] H. Sagawa, C. L. Bai, G. Colò, Phys. Scr. 91 (2016) 083011.
[19] B. D. Anderson, et al., Phys. Rev. C 27 (1983) 1387.
[20] I. J. van Heerden, et al., Phys. Rev. C 59 (1999) 1488.
[21] D. J. Mercer, et al., Phys. Rev. C 49 (1994) 3104.
[22] Y. Fujita, J. Phys.: Conf. Ser. 20 (2005) 107.
[23] T. Adachi, et al., Nucl. Phys. A 788 (2007) 70c.
[24] A. Tamii, et al., Nucl. Instr. and Meth. Phys. Res. A 605 (2009) 326.
[25] H. Matsubara, et al., Phys. Rev. Lett. 115 (2015) 102501.
[26] C. Djalali, G. M. Crawley, B. A. Brown, V. Rotberg, G. Caskey, A. Galonsky, N. Marty, M. Morlet, A. Willis, Phys. Rev. C 35 (1987) 1201.
[27] G. M.Crawley, C. Djalali, N. Marty, M. Morlet, A. Willis, N. Anantaraman, B. A. Brown, A. Galonsky, Phys. Rev. C 39 (1989) 311.
[28] Y. Fujita, et al., Phys. Rev. C 59 (1999) 90, and references therein.
[29] Y. Fujita, et al., Phys. Rev. C 62 (2000) 044314.
[30] H. J. Ong, et al., Phys. Lett. B 725 (2013) 277.
[31] I. Miura, et al., RCNP Annual Report 1991, Osaka University, p. 149.
[32] T. Wakasa, et al., Nucl. Instr. and Meth. Phys. Res. A 482 (2002) 79.
[33] H. Matsubara, et al., Nucl. Instr. Meth. A 678 (2012) 122.
[34] M. Fujiwara, et al., Nucl. Instr. and Meth. Phys. Res. A 422 (1999) 484.
[35] T. Noro, et al., RCNP Annual Report 1991, Osaka University, p. 177.
[36] H. Fujita, G. P. A. Berg, Y. Fujita, K. Hatanaka, T. Noro, E. J. Stephenson, C. C. Foster, H. Sakaguchi, M. Itoh, T. Taki, K. Tamura, , H. Ueno, Nucl. Instr. and Meth. Phys. Res. A 469 (2001) 55.
[37] H. Fujita, et al., RCNP Annual Report 2010, Osaka University, p. 3.
[38] Y. Shimbara, et al., Phys. Rev. C 86 (2012) 024312.
[39] D. R. Tilley, H. R. Weller, C. M. Cheves, R. Chasteler, Nucl. Phys. A 595 (1995) 1, and references therein.
[40] J. Cook and J. A. Carr, computer program FOLD/DWHI, Florida State University (unpublished), based on F. Petrovich and D. Stanley, Nucl. Phys. A 275 (1977) 487, modified as described in J. Cook *et al.*, Phys. Rev. 30 (1984) 1538 and R. G. T. Zegers, S. Fracasso and G. Colò, 2006 (unpublished).
[41] H. Fujita, et al., Phys. Rev. C 79 (2009) 024314.
[42] T. Yamagata, H. Utsunomiya, M. Tanaka, S. Nakayama, N. Koori, A. Tamii, Y. Fujita, K. Katori, M. Inoue, M. Fujiwara, H. Ogata, Nucl. Phys. A 589 (1995) 425.
[43] J.Kamiya, et al., Phys. Rev. C 67 (2003) 064612.
[44] Y. Shimbara, R. G. T. Zegers, H. Fujita, private communication (2005).
[45] S. van der Werf, S. Brandenburg, P. Grasdijk, W. A. Sterrenburg, M. Harakeh, M. Greenfield, B. A. Brown, M. Fujiwara, Nucl. Phys. A 496 (1989) 305.
[46] R. G. T. Zegers, et al., Phys. Rev. Lett. 99 (2007) 202501.
[47] A. T. Laffoley, et al., Phys. Rev. C 92 (2015) 025502.
[48] Y. Fujita, et al., Phys. Rev. C 59 (1999) 90.
[49] Y. Fujita, Y. Utsuno, H. Fujita, JPS Conf. Proc. 23 (2018) 012030.
[50] B. A. Brown, W. A. Richter, Phys. Rev. C 74 (2006) 034315.
[51] Y. Utsuno, S. Chiba, Phys. Rev. C 83 (2011) 021301(R).
[52] K. Yoshida, Prog. Theor. Exp. Phys. 2013 (2013) 113D02.
[53] N. V. Giai, H. Sagawa, Phys. Lett. B 106 (1981) 379.

TABLE I: Evaluated E_x and J^π values of states up to 6.3 MeV and the E_x and Rr_4 derived in the present analysis. For definition of the Rr_4 ratio, see text.

Evaluated values[a]		Present analysis	
E_x (MeV)	J^π	E_x (MeV)	Rr_4
0.000	1^+	0.000	1.0[b]
0.93720(6)	3^+	0.938	1.3
1.04155(8)	IAS, 0^+	1.043	1.2
1.70081(18)	1^+	1.701	1.1
3.06184(18)	2^+	3.063	1.9
3.72419(22)	1^+	3.725	1.3
3.83917(22)	2^+	3.840	1.5
4.36015(26)	1^+	4.361	1.0
5.60338(27)	1^+	5.602	1.9
5.60486(28)	1^-		
5.786(2)	2^-	5.791	> 10
6.0964(11)	4^-	6.099	> 5
6.108(3)	(1^+)		
6.262(3)	1^+	6.256	1.1

[a]From Ref. [39].
[b]Rr_4 ratio of this state is normalized to be one.

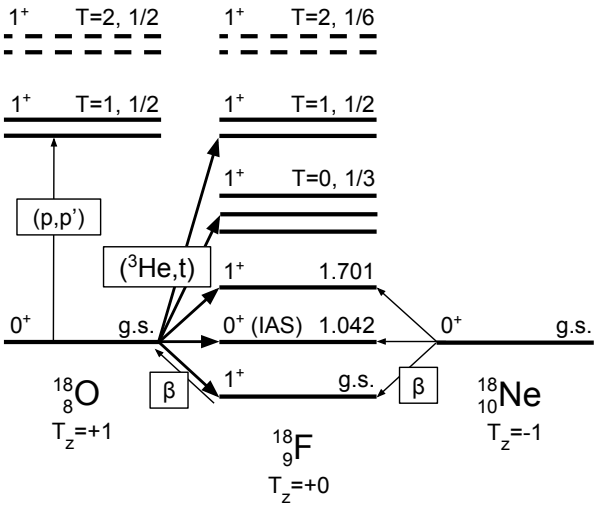

FIG. 1: Isospin structure of analogous GT and Fermi transitions among the $A = 18$ isobars ^{18}O, ^{18}F, and ^{18}Ne with $T_z = +1$, 0, -1, respectively. The J^π values, isospin T, and the squared values of the isospin Clebsch-Gordan coefficients are given for the representative states.

TABLE II: Evaluated E_x and J^π values, and natural decay width Γ for the states above 6.5 MeV and the E_x, Γ, Rr_4, and ΔL values derived in the present analysis. For the definition of ratio Rr_4, see text.

Evaluated values[a]			Present analysis			
E_x (MeV)	J^π	Γ (keV)	E_x (MeV)	Γ (keV)	Rr_4	ΔL
6.6437(8)	2^-	0.60(7)	6.66	30−50	> 10	≥ 1
6.647(4)	1^-	91(4)				
6.803(2)	$1^+, 2, 3^+$	< 2	6.81	80−90	> 5	≥ 1
6.809(5)	2^-	88(2)				
7.201(2)	(4^+)	6.5	7.22	40−50	> 5	≥ 1
7.247(2)	(1^+)	46.5				
7.406(2)	1^+	14.6(14)	7.42	20−30	2.3	(0)[b]
7.555(2)	(1^-)	30	7.59	70−80	> 5	≥ 1
7.584(2)		9(2)				
8.064(6)	≥ 4	60	8.06	140−160	> 10	≥ 1
8.209(2)	2^-	52	8.22	50−70	> 10	≥ 1
8.238(2)	4^+	20				
			8.34	150−220	> 5	≥ 1
			9.16	200−300	1.5	(0)
			9.65	170−230	0.75	(0)
			9.92	140−160	1.5	(0)
			10.9	400−600	1.5	(0)
			11.8	400−600	1.4	(0)

[a]From Ref. [39].
[b]See text.

TABLE III: The B(GT) values obtained from the present ^{18}O(^{3}He,t)^{18}F reaction, the ^{18}Ne β^+ decay [39, 47], the ^{18}O(p,n) reactions [19–21], and the $B(M1_\sigma)$ values from the ^{18}O(p,p') reaction data [26]. The B(GT) values from the (p,n) reactions [19–21] are renormalized using the present standard value from the ^{18}F β-decay data [39]. For the B(GT) values from Ref. [19], additional ambiguities of 5% were added due to the relative ambiguity of the 0° cross sections. The units of the transition strengths from the (p,p') data [26] are converted to those of the $B(M1_\sigma)$ values for the direct comparison. For details, see text.

Present data			^{18}Ne β-decay	(p,n)[a]			(p,n)[b]		(p,n)[c]	(p,p')	
E_x	B(GT,F)	T	B(GT,F)	E_x	B(GT)	T	E_x	B(GT)	B(GT)	E_x in ^{18}O	$B(M1_\sigma)$
g.s.	3.092(16)	0	3.123(24)	g.s.	3.092(16)	0	g.s.	3.092(16)	3.092(16)		
1.043 (IAS)	2	1	2.11(6)								
1.701	0.170(2)	0	0.131(5)	1.70	0.187(13)	0	1.70	0.21(2)			
3.725	0.173(2)	0		3.72	0.177(13)	0	3.72	0.19(2)			
4.361	0.090(2)	0		4.35	0.084(6)	0	4.35	0.09(1)			
5.602	< 0.01	0									
6.099	< 0.01	0									
6.256	0.069(1)	0		6.26	0.059(4)	0	6.11+6.26	0.08(1)			
7.42	< 0.01	0									
9.16	0.03(1)	0									
9.65	0.05(1)	0									
9.92	0.07(2)	1		9.9	0.056(4)	(1)	9.9	0.14(2)		8.82	0.07(1)
10.9	0.19(3)	1		10.9	0.084(6)	(1)	11.1	0.18(3)			
11.8	0.07(2)	1		11.9	0.061(4)	(1)	12.0	0.12(2)		10.10	0.31(4)
										12.4−15.0	
Total	4.06(5)				3.80(3)			4.10(5)	4.2(5)		

[a]At E_p=135 MeV [19].
[b]At E_p=118 MeV [20].
[c]At E_p=494 MeV [21].

TABLE IV: Deduced R^2 values for ^{18}O(^{3}He,t)^{18}F and ^{42}Ca(^{3}He,t)^{42}Sc measurements and the related parameters.

^{18}O			^{42}Ca		
	Counts ($\times 10^4$)	B(GT,F)	E_x (MeV)	Counts ($\times 10^4$)	B(GT,F)
g.s. (GT)	16.32(4)	3.092(16)	g.s. (IAS)	3.45(5)	2
1.043 (IAS)	1.629(13)	2	0.611 (GT)	24.10(11)	2.17(5)
		$R^2 = 6.45(6)$			$R^2 = 6.45(18)$

TABLE V: Obtained B(GT) values from the QRPA calculation applying a IS to IV strength ratio $f = 1.3$ for the lower-energy (LE) peak at $E_x = 4.05$ MeV, the tiny peak at 7.86 MeV, and the higher-energy (HE) peak at 12.4 MeV. The reduced matrix elements for each configuration are shown with the corresponding 2qp energy in MeV. Only those 2qp excitations possessing the RPA amplitude greater than 0.01 are shown. Note that the 2qp energies and E_x values are with respect to the ^{18}O ground state. For details of calculation, see text.

	$\nu d_{5/2} \rightarrow \pi d_{5/2}$	$\nu 2s_{1/2} \rightarrow \pi 2s_{1/2}$	$\nu d_{3/2} \rightarrow \pi d_{5/2}$	$\nu p_{1/2} \rightarrow \pi p_{1/2}$	$\nu d_{5/2} \rightarrow \pi d_{3/2}$	
E_x in ^{18}O (MeV)	5.50	10.0	10.8	11.4	12.2	B(GT)
4.05	0.754	0.063	0.103	-0.028	0.156	3.97
7.86	0.436	-0.138	-0.175	0.013	-0.291	0.16
12.4	-0.043	-0.043	-0.094		0.733	1.12

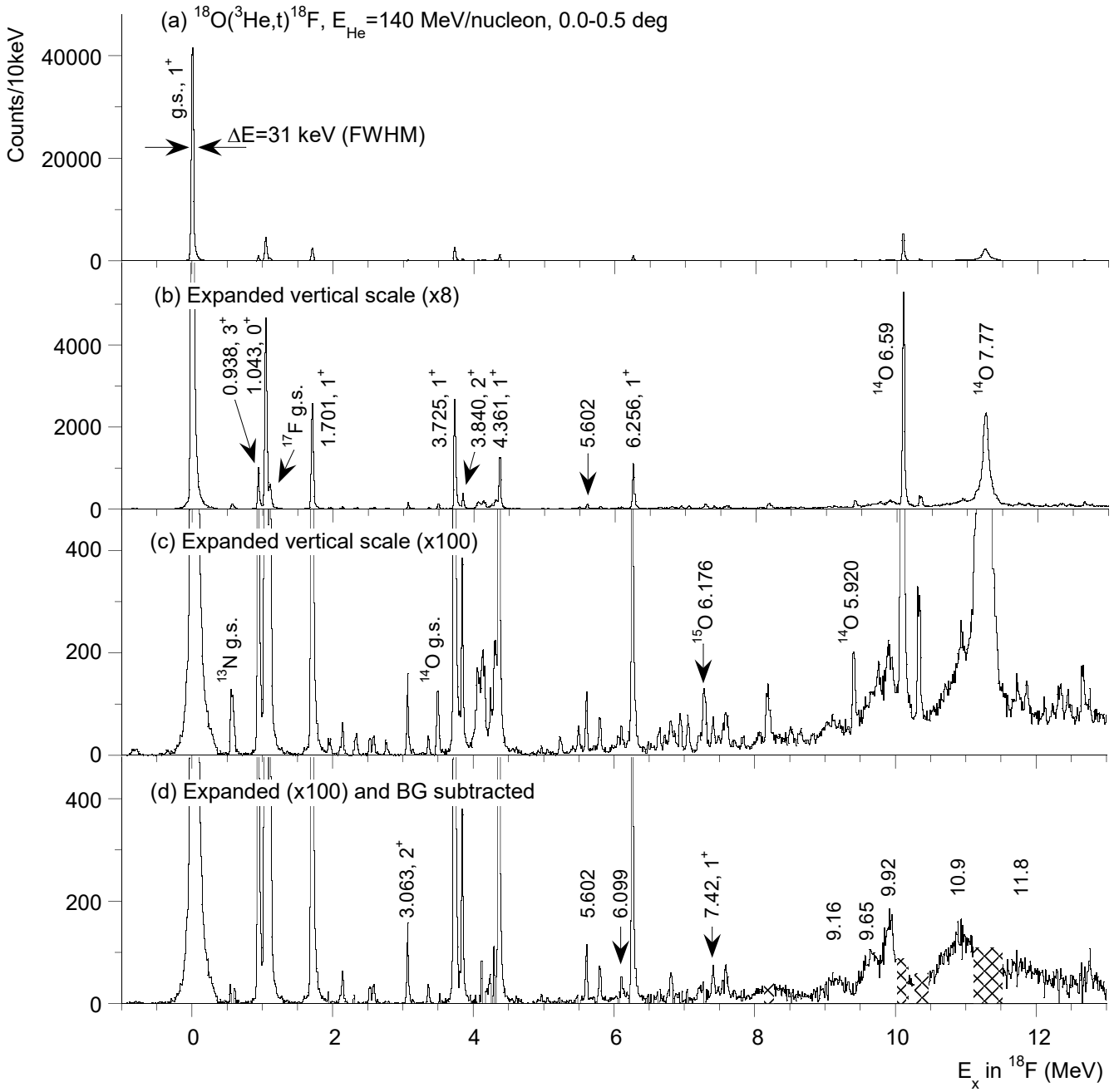

FIG. 2: Excitation energy spectra of ^{18}O(^{3}He,t)^{18}F measurements for scattering angles $0.0^\circ - 0.5^\circ$ (a) with full vertical scale, (b) with expanded scale (×8), (c) with more expanded scale (×100) before the background (BG) subtraction, and (d) with the same scele as (c) but after the BG subtraction. An energy resolution of 31 keV is achieved. For details, see text.

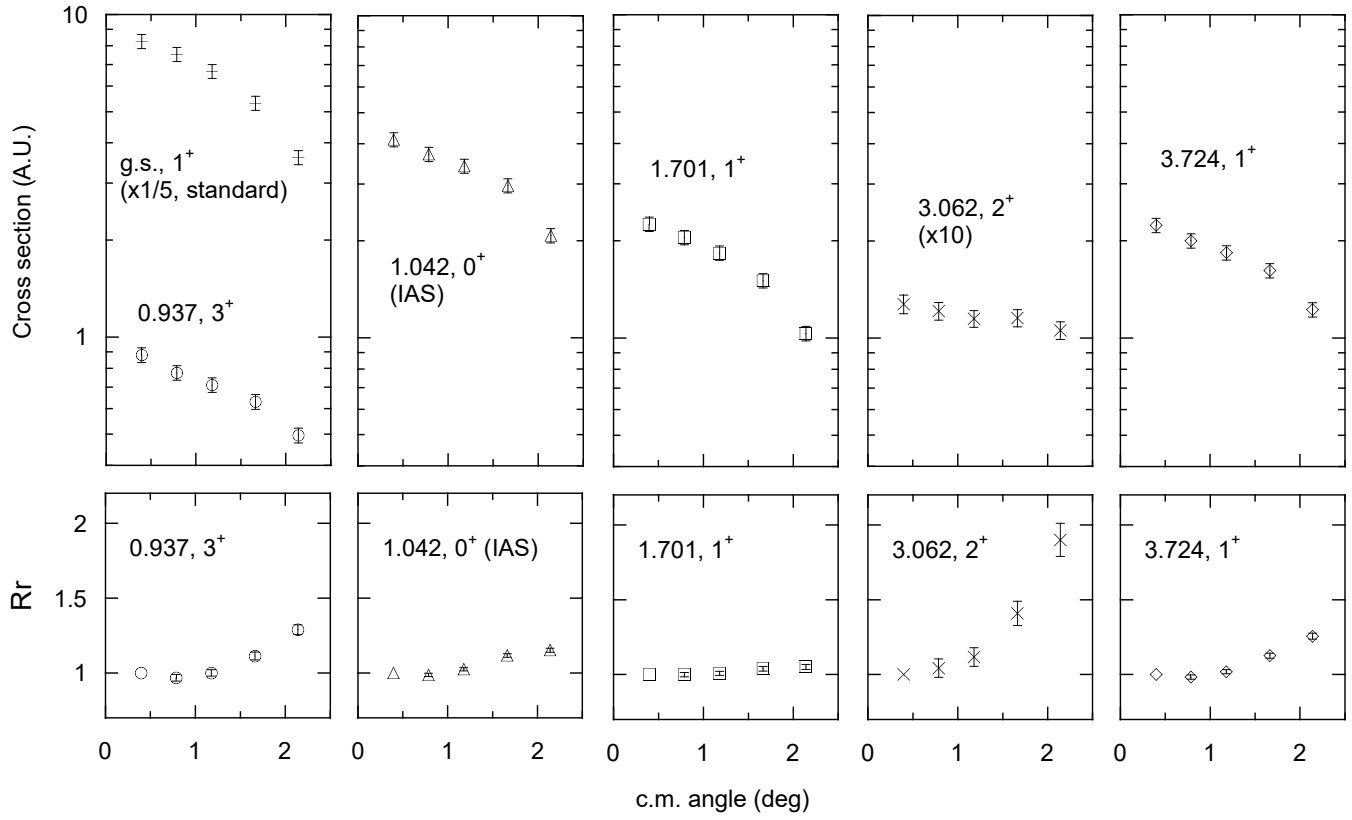

FIG. 3: Obtained angular distributions for the low lying states (top) and the corresponding Rr values (bottom). In the left-top panel, the angular distribution of the ^{18}F g.s., which is used as the standard for the derivation of Rr ratios, is also shown. For details, see text.

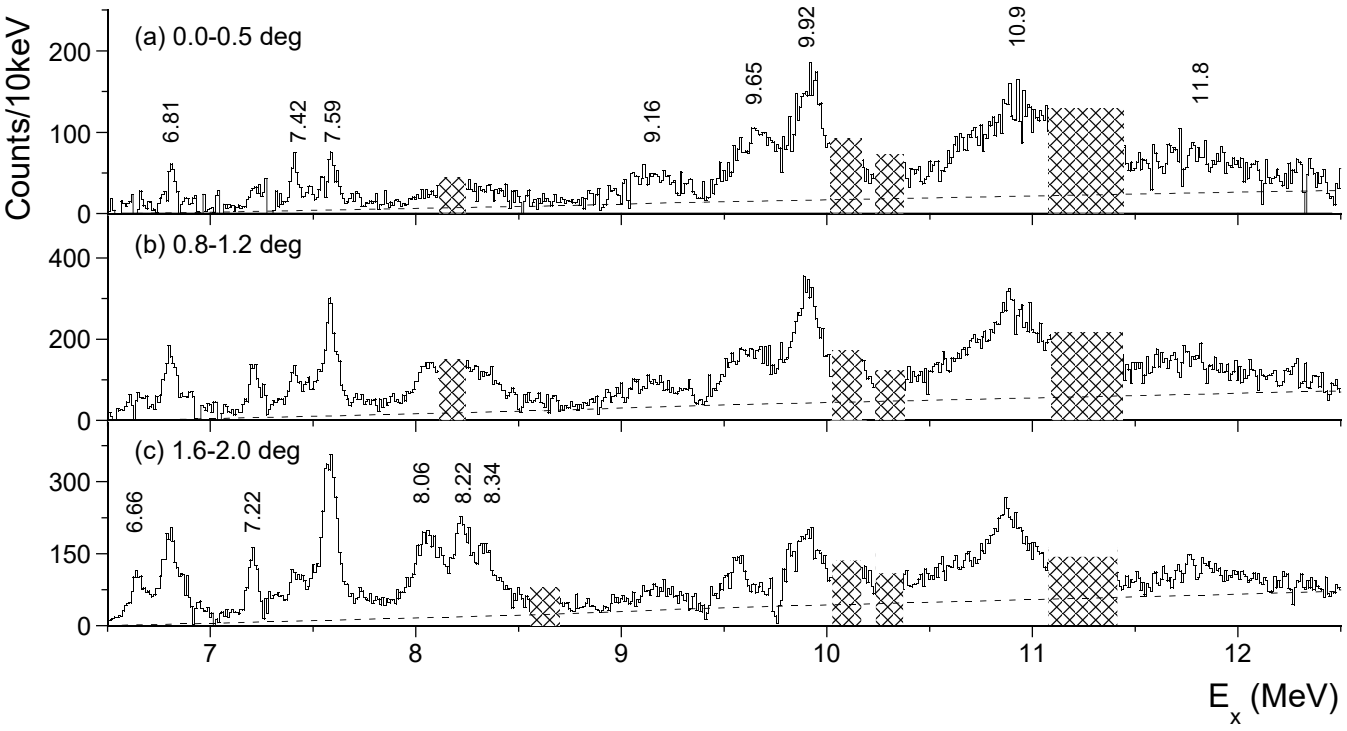

FIG. 4: The ^{18}O(^{3}He,t)^{18}F spectra in the energy region of $E_x = 6.5 - 12.5$ MeV for scattering angles (a) $0.0^\circ - 0.5^\circ$, (b) $0.8^\circ - 1.2^\circ$, and (c) $1.6^\circ - 2.0^\circ$. Vertical axes are normalized by the corresponding solid angles. Events from contaminating nuclei are subtracted in all the spectra. The regions where the spectra are distorted by the background subtraction are hatched. The dashed lines show the QFS continuum assumed in the peak decomposition analysis. For details, see text.

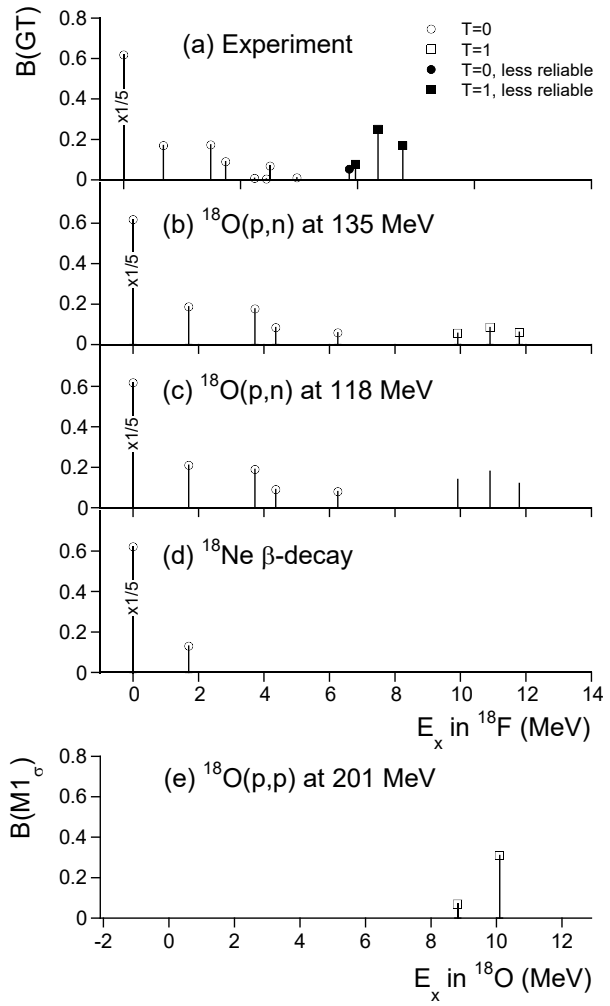

FIG. 5: The B(GT) strength distributions from (a) the present (^{3}He,t) data, (b) the (p,n) data at 135 MeV [19], (c) the (p,n) data at 118 MeV [20], (d) the ^{18}Ne β-decay [39, 47], and (e) the $B(\mathrm{M1}_\sigma)$ values from the (p,p') data at 201 MeV [26]. The g.s. strengths are divided by a factor of 5. The horizontal axis of (e) is shifted by 1.1 MeV, so that the analog states are expected to be aligned.

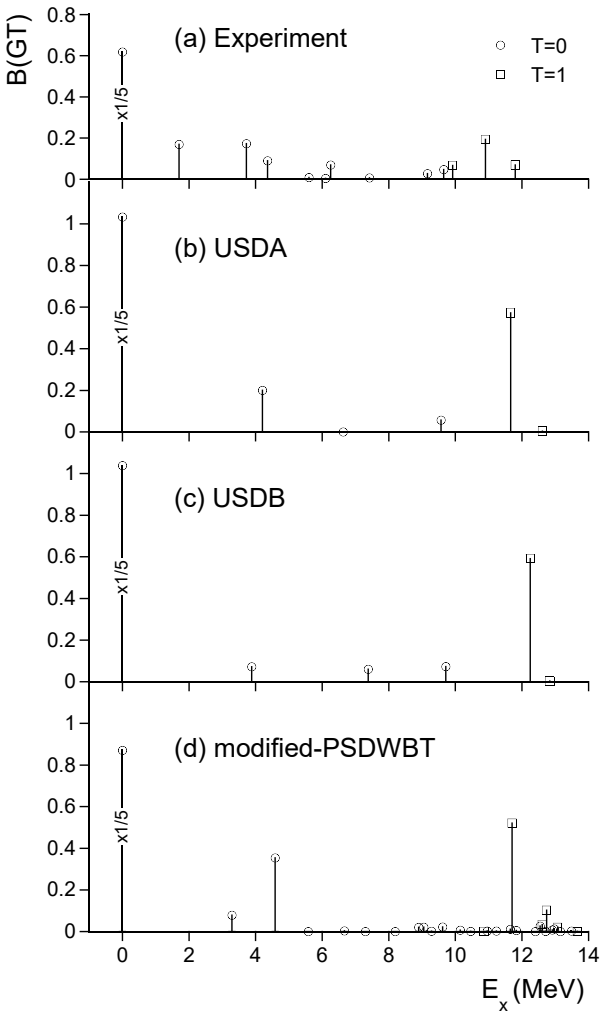

FIG. 6: The B(GT) strength distributions from (a) the present data and the Shell-Model calculations using the (b) USDA [50], (c) USDB [50], and (d) modified PSDWBT [51] interactions. The g.s. strengths are divided by a factor of 5.

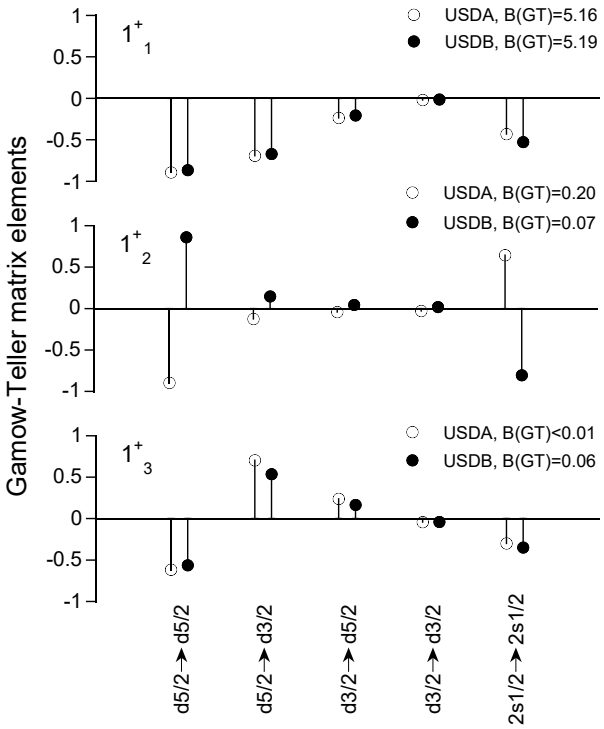

FIG. 7: The Gamow-Teller matrix elements for the three low-lying 1^+ states obtained by the USDA (open circle) and USDB (filled circle) interactions. The corresponding B(GT) values are shown together. For details, see text.

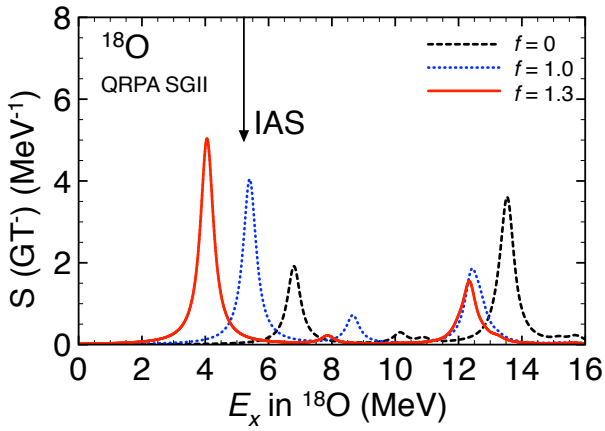

FIG. 8: Strength distributions of the ^{18}O $\rightarrow$ ^{18}F GT transitions obtained by the HFB + QRPA calculations employing the Skyrme SGII and the surface-type pairing interaction. The IS pairing interaction is included in the QRPA calculations with a factor f, a ratio of the strength for the IS pairing interaction to that for the IV pairing interaction. The arrow indicates the IAS obtained at $E_x = 5.14$ MeV.